Fibers and Polymers 2001, Vol.2, No.4, 203-211

Prediction and Measurement of Residual Stresses in Injection Molded Parts

Young Il Kwon, Tae Jin Kang, Kwansoo Chung, and Jae Ryoun Youn*

School of Materials Science and Engineering, Seoul National University, Seoul 151-742, Korea
(Received September 4, 2001; Revised October 5, 2001; Accepted October 7, 2001)

Abstract: Residual stresses were predicted by a flow analysis in the mold cavity and residual stress distribution in the injection molded product was measured. Flow field was analyzed by the hybrid FEM/FDM method, using the Hele Shaw approximation. The Modified Cross model was used to determine the dependence of the viscosity on the temperature and the shear rate. The specific volume of the polymer melt which varies with the pressure and temperature fields was calculated by the Tait's state equation. Flow analysis results such as pressure, temperature, and the location of the liquid-solid interface were used as the input of the stress analysis. In order to calculate more accurate gap-wise temperature field, a coordinate transformation technique was used. The residual stress distribution in the gap-wise direction was predicted in two cases, the free quenching and the constrained quenching, under the assumption that the shrinkage of the injection molded product occurs within the mold cavity and that the solid polymer is elastic. Effects of the initial flow rate, packing pressure, and mold temperature on the residual stress distribution was discussed. Experimental results were also obtained by the layer removal method for molded polypropylene.

Keywords: Injection molding, Residual stress, Hybrid FEM/FDM scheme, Layer removal method, Stephan problem

Introduction

Injection molding process is one of the most widely used methods to shape polymeric materials. Its application ranges from cups and toys to the home appliances and parts of airplanes. It is also one of the most important processes of polymeric materials, for it is not only due to its applicability but also its accuracy in shaping. The density of polymeric materials is very sensitive to temperature and pressure variations during molding, so the geometry of the final product is not the same as that of the cavity. Since physical properties are closely related to the distribution of the density in the product, it is possible that the product has such undesirable deformations as shirinkage, distorsion, warpage, voids, and so forth. It is important to predict the final shape and mechanical properties of the product, but it is very difficult because the product has complex geometry and the polymer melt shows viscoelastic properties. As the change in shape and mechanical properties of the final product are closely related to residual stresses in it, it is essential to predict the residual stress distribution in the final product for the production of precision parts.

Relation to Previous Work

The numerical analysis of the flow field in injection molding has been carried out by many reaserchers. Gilmore and Spencer[1,2] made a pioneering study to analyze the injection molding process a half century ago. Hieber and Shen[3] made systematic analysis on the filling stage by making use of the hybrid FEM/FDM scheme. Studies on the post-filling stage focused on the density change and carried out the analysis in a separate way from the filling stage analysis. Chiang *et al.*[4,5] developed a technique which could analyze the filling and post-filling stage at the same time.

Prediction of the residual stresses have been considered with only thermal effect in early years, but Zoetelief *et al.*[6] commented on the necessity of considering the pressure history in the molding process. He investigated the influence of the holding stage on the residual thermal stress distribution and Jansen and Titomanlio[7,8] studied the effect of in-mold shrinkage on residual stress distrbutions but did not carry out the flow field analysis.

Recently flow field analysis and residual stress analysis are being combined together and results of the flow analysis are used to predict the residual stress or shrinkage of the final product. Chiang *et al.*[4,5] employed a coupled analysis of the fluid flow and heat transfer in the polymer melt during filling, packing, and cooling stages which occured consecutively during the entire molding process. The results were used as the input for predicting shringkage and warpage. Kabanemi *et al.*[9] employed the thremoviscoelastic model with volume relaxation for the shirinkage analysis.

Destructive and non-destructive methods could be adopted in evaluation of the residual stress in the injection molded product. Since Trueting and Read[10] developed the technique to estimate the residual stresses in the specimen by measuring the curvature after successive removal of layers, it became the most generally used strategy in measuring the residual stresses and many research groups used the layer-removal method[11-16]. Jansen *et al.*[17] recently used an excimer laser to remove the successive layers.

In this study, the residual stress distribution in semi-crystalline material was predicted using the results of the flow field analysis. The non-Newtonian viscosity was described

*Corresponding author: jaeryoun@gong.snu.ac.kr

by the modified Cross model and the compressibility of the material was considered by using the Tait's state equation. The pressure field was predicted by a finite element method in which the Hele-shaw approximation was implemented. The temperature field in the gap-wise direction was obtained by the finite difference method using coordinate transfomation to consider the moving solid-melt interface. The residual stress in the gap-wise direction was predicted from the calculated pressure and temperature field in two cases, the free quenching and the constrained quenching. The residual stress profiles were compared with the experimental results. The layer-removal method was applied and the curvature data was used to calculate the residual stress distribution in the injection molded product by the formula proposed by Treuting and Read[10] where the material was assumed to be elastic.

Theoretical Modeling

Flow Analysis

Pressure Field

The generalized Hele-Shaw (GHS) flow and the lubrication approximation were considered for a thin cavity of planar geometry. For calculation of the temperature field, phase change was assumed to occur at the crystallization temperature of the semi-crystalline polymers with temperature being dependent on pressure. As the previous approach for this problem[3-5], governing equations for the flow field and temperature field for liquid and solid phase can be given by the following equations.

Continuity equation:

$$\frac{\partial \rho}{\partial t} + \frac{\partial}{\partial x}(\rho u) + \frac{\partial}{\partial y}(\rho v) + \frac{\partial}{\partial z}(\rho w) = 0 \tag{1}$$

Momentum equations:

$$\frac{\partial}{\partial z}\left(\eta \frac{\partial u}{\partial z}\right) - \frac{\partial p}{\partial x} = 0 \tag{2}$$

$$\frac{\partial}{\partial z}\left(\eta \frac{\partial v}{\partial z}\right) - \frac{\partial p}{\partial y} = 0 \tag{3}$$

Energy equations:

$$\rho C_{pl}\left(\frac{\partial T}{\partial t} + u\frac{\partial T}{\partial x} + v\frac{\partial T}{\partial y}\right) = k_l \frac{\partial^2 T}{\partial z^2} + \eta \dot{\gamma}^2 \tag{4}$$

$$\rho C_{ps} \frac{\partial T}{\partial t} = k_s \frac{\partial^2 T}{\partial z^2} \tag{5}$$

where x and y are the planar coordinates and z is the gapwise coordinate, while u, v, and w are the velocity components in the x, y, and z directions with t the time, p the pressure, T the temperature, C_p the specific heat, and k the thermal conductivity of the material with subscripts l and s denoting the liquid and solid phase, respectively. $\rho(T, p)$ is the density and $\eta(\dot{\gamma}, T, p)$ the shear viscosity, where $\dot{\gamma}$ is the shear rate,

$$\dot{\gamma} = \sqrt{\left(\frac{\partial u}{\partial z}\right)^2 + \left(\frac{\partial v}{\partial z}\right)^2} \tag{6}$$

The following interfacial energy balance equation should be applied at the liquid-solid boundary

$$\left[k_s \frac{\partial T_s}{\partial z} - k_l \frac{\partial T_l}{\partial z}\right]_{z=\delta} = \rho_s L \frac{\partial \delta}{\partial t} \tag{7}$$

where δ is the distance of the solid-liquid interface from the center of the thickness and L is the latent heat of the material. Other boundary conditions in the gapwise direction can be given as follows

$$u = v = w = 0;\ T = T_w \text{ at } z = h \tag{8}$$

$$\frac{\partial u}{\partial z} = \frac{\partial v}{\partial z} = \frac{\partial T}{\partial z} = 0;\ w = 0 \text{ at } z = 0 \tag{9}$$

where h denotes the half-gap thickness and T_w the constant wall temperature. Integrating equations (2) and (3) in the gapwise direction gives

$$\frac{\partial u}{\partial z} = -\frac{\Lambda_x z}{\eta};\ \frac{\partial v}{\partial z} = -\frac{\Lambda_y z}{\eta} \tag{10}$$

where

$$\Lambda_x = -\frac{\partial p}{\partial x};\ \Lambda_y = -\frac{\partial p}{\partial y}. \tag{11}$$

Combined with equation (6), it follows that

$$\dot{\gamma} = \frac{\Lambda z}{\eta} \tag{12}$$

where

$$\Lambda \equiv |\nabla p| = \sqrt{\left(-\frac{\partial p}{\partial x}\right)^2 + \left(-\frac{\partial p}{\partial y}\right)^2}. \tag{13}$$

Integrating equation (10) in the z direction and applying the boundary conditions given by the equation (8), it becomes

$$u = \Lambda_x \phi;\ v = \Lambda_y \phi \tag{14}$$

where

$$\phi \equiv \int_z^h \frac{\tilde{z}}{\eta} d\tilde{z}. \tag{15}$$

Then, the mass flow rate per unit length with respect to x and y can be obtained by integrating equation (14)

$$\dot{m}_x \equiv 2\int_0^h \rho u dz \equiv 2\tilde{S}\Lambda_x;\ \dot{m}_y = 2\int_0^h \rho v dz \equiv 2\tilde{S}\Lambda_y \tag{16}$$

where

$$\tilde{S} \equiv \int \rho \phi dz \tag{17}$$

is a measure of the fluidity.

Integrating equation (1) in the gapwise direction, the last

term on the left-hand side disappears due to the conditions on w in equations (8) and (9) and the time derivative in the first term can be moved to outside of the integral since $h(x, y)$ is independent of t, resulting in

$$2\frac{\partial}{\partial t}\int_0^h \rho dz + \frac{\partial}{\partial x}(\dot{m}_x) + \frac{\partial}{\partial y}(\dot{m}_y) = 0 \tag{18}$$

Substituting equation (16) into equation (18) and further decomposing the first term on the left-hand side of equation (18) by introducing the pressure and temperature dependence of ρ and allowing a possible discontinuity in the case of a semicrystalline polymer, the final governing equation can be obtained as follows.

$$G\frac{\partial P}{\partial t} - \frac{\partial}{\partial x}\left(\tilde{S}\frac{\partial P}{\partial x}\right) - \frac{\partial}{\partial y}\left(\tilde{S}\frac{\partial P}{\partial y}\right) = -F \tag{19}$$

where

$$G = \int_0^{\chi}\left(\frac{\partial \rho_l}{\partial P}\right)_T dz + \int_{\chi}^{h}\left(\frac{\partial \rho_s}{\partial P}\right)_T dz \tag{20}$$

$$F = \int_0^{\chi}\left(\frac{\partial \rho_l}{\partial T}\right)_P \frac{\partial T}{\partial t} dz + \int_{\chi}^{h}\left(\frac{\partial \rho_s}{\partial T}\right)_P \frac{\partial T}{\partial t} dz + (\rho_l - \rho_s)_{z=\chi}\frac{\partial \chi}{\partial t} \tag{21}$$

χ is the position of the solid-melt interface.

The modified cross model was used.

$$\eta = \frac{\eta_0}{1 + \left[\frac{\eta_0 \dot{\gamma}}{\tau^*}\right]^{1-n}} \tag{22}$$

where n is power-law index ($0.1 \le n \le 0.4$), η_0 is zero shear rate viscosity which is a function of the temperature and pressure and τ^* is the stress value which indicates the approximate transition region between the Newtonian fluid and the power-law fluid. The intrinsic viscosity which is a function of temperature and pressure is expressed as the following WLF type 7-constant viscous model which is known as valid for semi-crystalline materials in a wide range[4].

$$\eta_0(T, P) = D_1 \exp\left\{-\frac{A_1[T - T^*(P)]}{A_2 + D_3 P + [T - T^*(P)]}\right\} \tag{23}$$

where

$$T^*(P) = D_2 + D_3 P \tag{24}$$

The Tait state equation is used in order to consider the compressibility and the phase transition of the polymer. In the case of negative pressure, the pressure was set to be zero [4].

$$v(T, P) = v_0(T)\left[1 - C\ln\left(1 + \frac{P}{B(T)}\right)\right] \tag{25}$$

where C has the value of 0.0894, v is the specific volume, and

$$v_0(T) = \begin{cases} b_{1,l} + b_{2,l}\bar{T} & (T > T_t) \\ b_{1,s} + b_{2,s}\bar{T} & (T < T_t) \end{cases} \tag{26}$$

$$B(T) = \begin{cases} b_{3,l}\exp(-b_{4,l}\bar{T}) & (T > T_t) \\ b_{3,s}\exp(-b_{4,s}\bar{T}) & (T < T_t) \end{cases} \tag{27}$$

where

$$\bar{T} \equiv T - b_5 \tag{28}$$

Transition temperature is modeled as the linear function of the pressure which is melting temperature for semi-crystalline materials and glass transition temperature for amorphous materials.

$$T_t(P) = b_5 + b_6 P \tag{29}$$

The parameters used in the above equations are taken from the results of the previous research[18-21].

Boundary conditions for the polymer melt flow can be set as follows. The mass flow rate entering the mold, $\dot{m}_e$, was assumed to be constant at the entrance in the filling stage on the exit of cavity, C_e.

$$\dot{m} = \dot{m}_e \text{ on } C_e \tag{30}$$

The pressure at the inlet, p_e, was fixed in the holding stage.

$$p = p_e(t) \text{ on } C_e \tag{31}$$

There is no inward mass flow rate at the entrance in the cooling stage.

$$\dot{m} = 0 \text{ on } C_e \tag{32}$$

The pressure at the flow front is identical to the atmospheric pressure. Because the flux across the mold wall does not exist, the pressure gradient in normal direction is zero at wall boundaries.

$$\frac{\partial p}{\partial n} = 0 \text{ on } C_o, C_i \tag{33}$$

where C_o and C_i is the outer boundary of the cavity and the boundary of the insert respectively.

Temperature Field

The injection molded parts generally have the thin plate geometry, so the conduction in the thickness direction and the convection in the horizontal direction are considered only. The semicrystalline material used in this study, polypropylene, has two phase during injection molding and the solid-melt interface is moving as the polymer melt is solidified. The problem of this type, Stephan problem, can be dealt with by various techniques[22]. In this study, the fixed boundary method was applied in which the solid and liquid phases are equally divided respectively and as the interface moves to the center, the nodal point also moves. For the nodal point is moving as time passes, the

temperature value in the new position should be calculated. The coordinate transfomation was used to determine the temperature at the new nodal point. The energy equations (4) and (5) can be rewritten as follows, for liquid phase

$$\frac{\partial T_l}{\partial t} + u\frac{\partial T_l}{\partial x} + v\frac{\partial T_l}{\partial y} = \frac{k_l}{c_l\rho_l}\frac{\partial^2 T_l}{\partial z^2} + \frac{\eta_l}{c_l\rho_l}\dot{\gamma}^2 \tag{34}$$

and for solid phase

$$\frac{\partial T_s}{\partial t} = \frac{k_s}{c_s\rho_s}\frac{\partial^2 T_s}{\partial z_2} \tag{35}$$

The energy balance at the solid-melt interface equation (7) can be rewritten.

$$k_s\frac{\partial T_s}{\partial z} - k_l\frac{1}{\delta}\frac{\partial T_l}{\partial z} = L\rho\frac{d\delta}{dt} \tag{36}$$

The boundary and the initial conditions are written as follows.

$$\frac{\partial T}{\partial z} = 0 \text{ at } z = 0 \tag{37}$$

$$T_s = T_l = T_m \text{ at } z = \delta(t) \tag{38}$$

$$T_s = T_{wall} \text{ at } z = h \tag{39}$$

$$T = T_0(z) \text{ at } t = 0 \tag{40}$$

New coordinates are defined as follows,

$$\zeta_l = \frac{z}{\delta(t)},\ \zeta_s = \frac{z-h}{\delta(t)} \tag{41}$$

then we can obtain the derivatives of new coordinates with respect to the old coordinate and time.

$$\frac{\partial\zeta_l}{\partial z} = \frac{1}{\delta(t)},\ \frac{d\zeta_s}{dz} = -\frac{1}{h-\delta(t)} \tag{42}$$

$$\frac{\partial\zeta_l}{\partial t} = -\frac{z}{\delta^2}\frac{d\delta}{dt},\ \frac{\partial\zeta_s}{\partial t} = \frac{h-z}{(h-\delta)^2}\frac{d\delta}{dt} \tag{43}$$

The derivatives of temperature are also expressed as below.

$$\left.\frac{\partial T_l}{\partial t}\right|_z = \frac{\partial T_l}{\partial\zeta_l}\frac{\partial\zeta_l}{\partial t} + \left.\frac{\partial T_l}{\partial t}\right|_{\zeta_l} = -\frac{z}{\delta^2}\frac{d\delta}{dt}\frac{\partial T_l}{\partial\zeta_l} + \left(\frac{\partial T_l}{\partial t}\right)_{\zeta_l} \tag{44}$$

$$\left.\frac{\partial T_s}{\partial t}\right|_z = \frac{\partial T_s}{\partial\zeta_s}\frac{\partial\zeta_s}{\partial t} + \left.\frac{\partial T_s}{\partial t}\right|_{\zeta_s} = \frac{h-z}{(h-\delta)^2}\frac{d\delta}{dt}\frac{\partial T_s}{\partial\zeta_s} + \left(\frac{\partial T_s}{\partial t}\right)_{\zeta_s} \tag{45}$$

$$\frac{\partial T_l}{\partial z} = \frac{\partial T_l}{\partial\zeta_l}\frac{\partial\zeta_l}{\partial z} = \frac{1}{\delta}\frac{\partial T_l}{\partial\zeta_l} \tag{46}$$

$$\frac{\partial T_s}{\partial z} = \frac{\partial T_s}{\partial\zeta_s}\frac{\partial\zeta_s}{\partial z} = \frac{-1}{h-\delta}\frac{\partial T_s}{\partial\zeta_s} \tag{47}$$

$$\frac{\partial^2 T_l}{\partial z^2} = \frac{\partial}{\partial\zeta_l}\left(\frac{\partial T_l}{\partial z}\right)\frac{\partial\zeta_l}{\partial z} = \frac{1}{\delta^2}\frac{\partial^2 T_l}{\partial\zeta_l^2} \tag{48}$$

$$\frac{\partial^2 T_s}{\partial z^2} = \frac{\partial}{\partial\zeta_s}\left(\frac{\partial T_s}{\partial z}\right)\frac{\partial\zeta_s}{\partial z} = \frac{1}{(h-\delta)^2}\frac{\partial^2 T_s}{\partial\zeta_s^2} \tag{49}$$

Then the following governing equation can be obtained by applying above relationships for liquid phase

$$\left(\frac{\partial T_l}{\partial t}\right)_{\zeta_l} - \frac{z}{\delta^2}\frac{d\delta}{dt}\frac{\partial T_l}{\partial\zeta_l} + u\frac{\partial T_l}{\partial x} + v\frac{\partial T_l}{\partial y} = \frac{k_l}{c_l\rho_l}\frac{1}{\delta^2}\frac{\partial^2 T_l}{\partial\zeta_l^2} + \frac{\eta_l}{c_l\rho_l}\dot{\gamma}^2 \tag{50}$$

and for solid phase.

$$\left(\frac{\partial T_s}{\partial t}\right)_{\zeta_s} + \frac{h-z}{(h-\delta)^2}\frac{d\delta}{dt}\frac{\partial T_s}{\partial\zeta_s} = \frac{k_s}{c_s\rho_s}\frac{1}{(h-\delta)^2}\frac{\partial^2 T_s}{\partial\zeta_s^2} \tag{51}$$

The solid-melt interface moves by obeying the energy balance at that position:

$$-k_s\frac{1}{h-\delta}\frac{\partial T_s}{\partial\zeta_s} - k_l\frac{1}{\delta}\frac{\partial T_l}{\partial\zeta_l} = L\rho\frac{d\delta}{dt} \tag{52}$$

The boundary and initial conditions are converted as follows in the new coordinate system.

$$\frac{\partial T_l}{\partial\zeta_l} = 0 \text{ at } \zeta_l = 0 \tag{53}$$

$$T_s = T_l = T_m \text{ at } \zeta_l = \zeta_s = 1 \tag{54}$$

$$T_s = T_{wall} \text{ at } \zeta_s = 0 \tag{55}$$

$$T = T_0 \text{ at } t = 0 \tag{56}$$

Prediction of the Residual Stress

The formula, equation (57), proposed by Jansen[7] is used to predict the residual stress distribution in the final polymer product. The solid polymer is assumed to be elastic, while the melt is considered to be unable to withstand relevant tensile stresses, and the normal stress, σ_{zz}, is thought to be independent of z. If the shrinkage can be prevented before ejection by either interaction forces at the mold wall which is presented by the superscript *IM*0' or geometrical constraints, the following equation can be used to predict the in-plane stress in the injection molded part after ejection. P_s means the pressure when the polymer is solidified, ε^i_{xx} contains all the strains excluding the components due to the pressure and bar means the thickness averaged properties.

$$\sigma^{IM0'}_{xx}(z,t) = -K[P_s - \bar{P}_s] + \frac{E}{1-\nu}[\bar{\varepsilon}^i_{xx}(t) - \varepsilon^i_{xx}(z,t)] \tag{57}$$

Bulk modulus of the material K has the following relationship

$$K = \frac{\beta E}{1-\nu} = \frac{1-2\nu}{1-\nu}, \tag{58}$$

where P is the pressure and subscript s refers to solidification, β is the linear compressibility, E is the Young's Modulus, and ν is the Poisson's ratio. The last term of the equation (57) will vanish for the constant final temperature.

If there is no friction between the solidified polymer and the mold wall, the polymer can shrink freely during cooling, which gives free quenching condition.

Experimental

The specimen was made by using a closed circuit injection molding machine. The diameter of the screw is 50 mm, and a commercially available polypropylene (HYUNDAI SEETEC PP H1500) was used. The mold has a cavity of rectangular plate(200×40×3 mm), triangular inlet, trapezoidal runner, and conical sprue, as shown in Figure 1. schematically. The mesh used in simulation is shown in Figure 2. Processing conditions were set as follows. The mold temperature was 30°C, the barrel temperature was 210°C, filling time was 8 seconds, and cooling time was 21 seconds. The material constants are shown in Tables 1 to 4. The ejected parts were cut by a jigsaw along the dotted line shown in Figure 1(80× 22×3 mm^3) and the samples were used to determine the residual stress of the product. Residual stresses were measured by using the layer removal procedure. It involves removing thin uniform layers from one surface of the specimen and measuring the curvature change that results from the consequent change in the stress distribution after each removal of layers. Layers were removed by a high speed milling machine using a single point cutter and fly-cutting action. The specimen was attached to a gauge block with a double sticking tape and cut at the speed of 1220 rpm. The thickness and the arc length of the specimen was measured by a micrometer and a pair of calipers. The image of the specimen was obtained by image scanning and its curvature was calculated by assuming that the curved specimen be a part of a perfect circle. The residual stress distribution was obtained with respect to depth from the

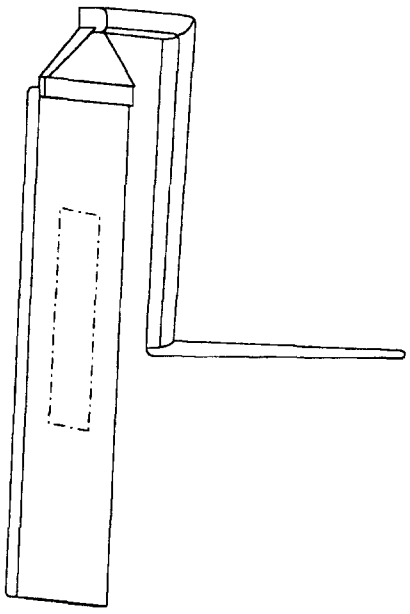

Figure 1. Schematic diagram of the mold used for the experiment (the specimen was prepared by cutting along the dotted line).

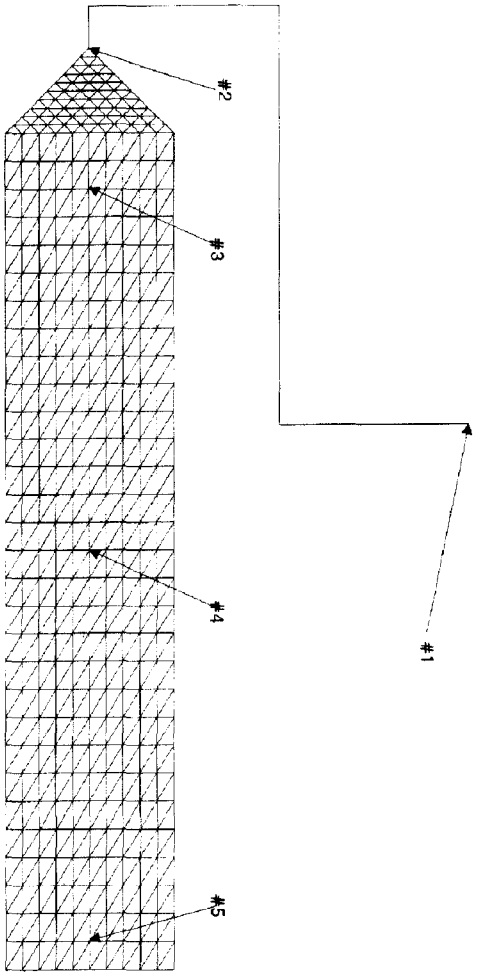

Figure 2. Finite element mesh and positions of interes.

Table 1. Cross 5-constant model constants for PP

n	0.204
τ^* (Pa)	3.07×10^4
B (Pa · s)	0.144
Tb (K)	4830
β (Pa^{-1})	4.39×10^{-9}

Table 2. Specific-volume model constants for PP

$b_{1,l}$ (m^3/kg)	1.3193×10^{-3}
$b_{2,l}$ (m^3/kg °C)	1.1563×10^{-6}
$b_{3,l}$ (Pa)	6.617×10^7
$b_{4,l}$ ($°C^{-1}$)	0.7557×10^{-3}
$b_{1,s}$ (m^3/kg)	1.2304×10^{-3}
$b_{2,s}$ (m^3/kg °C)	7.64×10^{-7}
$b_{3,s}$ (Pa)	9.7292×10^7
$b_{4,s}$ ($°C^{-1}$)	2.4623×10^{-3}
b_5 (°C)	118.0
b_6 (°C/Pa)	2.25×10^{-7}

Table 3. Thermal properties of PP

C_{pl} (J/kg · K)	2.7×10^3
C_{ps} (J/kg · K)	2.0×10^3
k_l (W/m · K)	0.175
k_s (W/m · K)	0.22
L (J/kg)	2.34×10^5

Table 4. Elastic modulus and Poisson's ratio of PP

E (MPa)	1032
ν	0.4

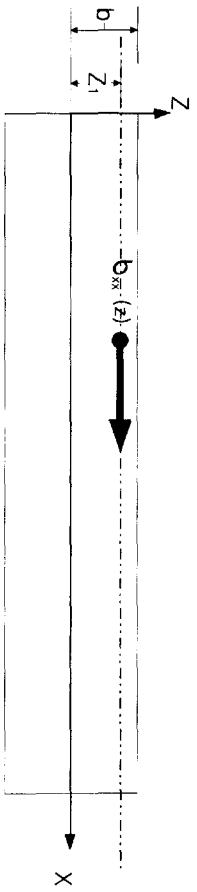

Figure 3. Schematic representation of the layer removal method.

curvature variation after each layer removal. The measured curvature, ρ, was then plotted with respect to the depth of material removed, $(b - z_l)$, where $2b$ is the initial thickness and z_l is the distance from the neutral plane to the new machined surface, as shown in Figure 3.

Assuming that the thermal contraction is isotropic and the curvature is the same in all directions, the residual stress distribution was determined by using the equation provided by Treuting and Read[10]:

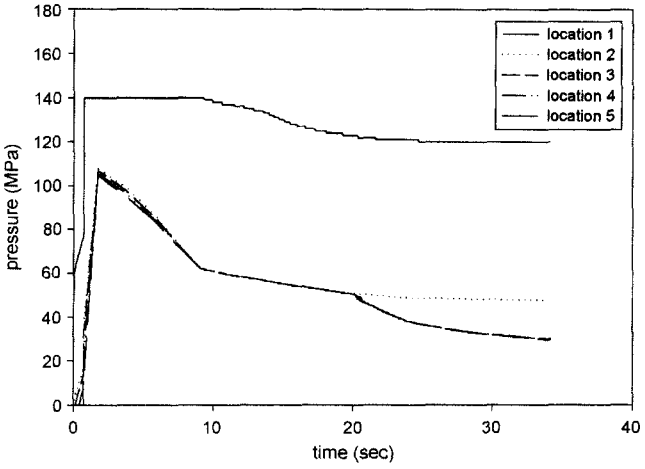

Figure 4. Predicted pressure variation in the mold as a function of time when the flow rate is 42 cm^3/s, packing pressure is 140 MPa, and mold temperature is 40°C.

$$\sigma_x(z_l) = \frac{-E}{6(1-\nu)}\left\{(z_l+b)^2\frac{d\kappa_x(z_l)}{dz_l} + 4(z_l+b)\kappa_x(z_l) - 2\int_{z_l}^{b}\kappa_x(z)dz\right\} \quad (59)$$

where χ_k is the curvature in the x direction, E is the Young's modulus, and ν is the Poisson's ratio. If the specimen is curved before the layer removal the initial curvature is subtracted from each of the subsequent measured curvature before performing the Treuting and Read analysis.

Results and Discussion

Effects of initial inward mass flow rate at the gate, packing pressure, and mold temperature on the residual stress was examined. The pressure variation with respect to time is shown in Figure 4 where the flow rate was 42 cm^3/s, the packing pressure was 140 MPa, and the mold temperature was 40°C. During filling stage, pressure increased linearly and after complete filling high constant pressure was maintained at the sprue in packing stage. Although the constant pressure was maintained at the sprue, the pressure in the mold cavity dropped during packing. It was believed that the the pressure was reduced to compensate for the shrinkage due to cooling of the polymer resin. After the packing (at about 8 seconds), the cooling step began, where the mass flow through the gate was assumed to be zero. The pressure changed in about 20 seconds when the polymer was solidified completely. The pressure decreased almost at constant rate as the temperature decreased in the cavity for 20 seconds, while the slope became larger abruptly after that time. As polypropylene is a semi-crystalline polymer, the density of which increases at melting temperature. The effect of cooling on the pressure is reflected by the reduction of the specific volume before the complete solidification of the

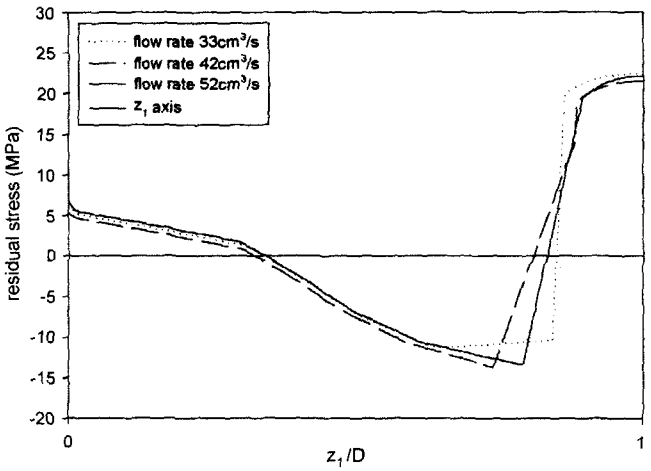

Figure 5. Predicted residual stress distribution for various flow rates when packing pressure is 140 MPa and temperature is 40°C.

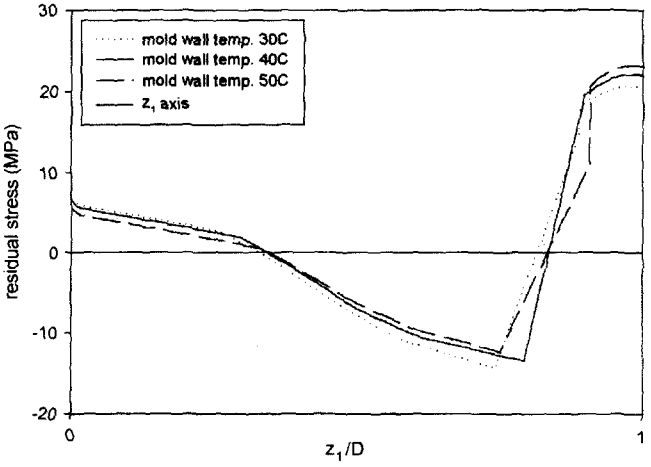

Figure 7. Predicted residual stress distribution for various mold wall temperature when flow rate is 52 cm^3/s, and packing pressure is 140 MPa.

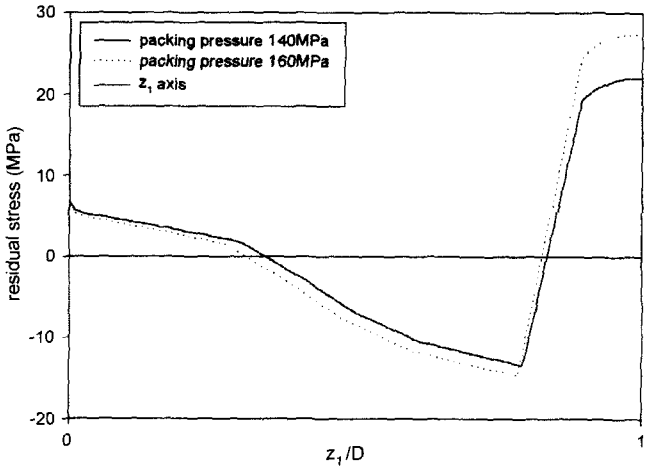

Figure 6. Predicted residual stress distribution for different packing pressure when flow rate is 52 cm^3/s and temperature is 40°C.

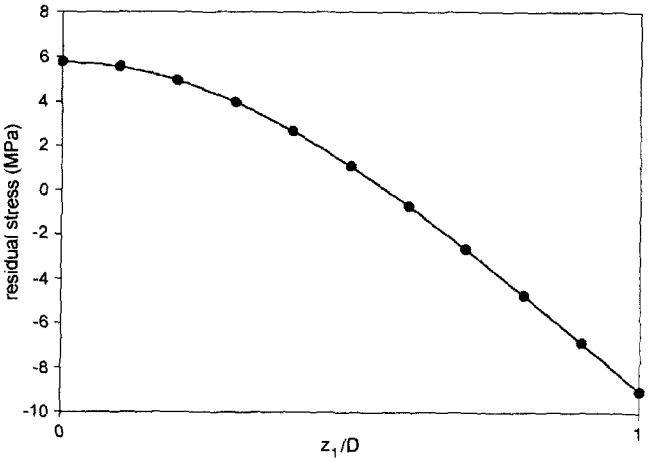

Figure 8. Predicted residual stress profile at the center of the product assuming the free boundary condition.

polymer and the temperature decrease causes the pressure drop after the solidification.

The residual stress distribution in the polymer product was calculated asssuming perfect adhesion at the cavity wall and the result was plotted with respect to the gapwise direction in Figure 5 for various flow rates. As reported by other research groups[11-16], tensile residual stress is developed in the core and at the surface region and the compressive stress in the intermediate region. The effect of the initial inward flow rate on the residual stress distribution was shown in the figure. The size of the tensile stress region at the surface is affected by the duration of the filling stage. In other words, the longer the filling time, the broader the tensile region at the surface. The effect of the magnitude of the packing pressure on the residual stress is presented in Figure 6. The increase in the packing pressure results in the increase of residual stress, which can be recognized directly from the figure, but the shape of the profile changed slightly. At large packing pressure, more material could be placed in the mold and its density became larger and the residual stress also increased. The effect of the mold temperature on the residual stress distribution was shown in Figure 7. It is observed that the colder the mold wall, the larger the tensile region. At low mold wall temperature, the polymer melt cools more rapidly and the tensile region can grow larger than that at high mold wall temperature.

The residual stress distribution in the case of free quenching is predicted in Figure 8. The graph can be divided to two regions; tensile core region and compressive surface region. The experimentally measured curvature and the

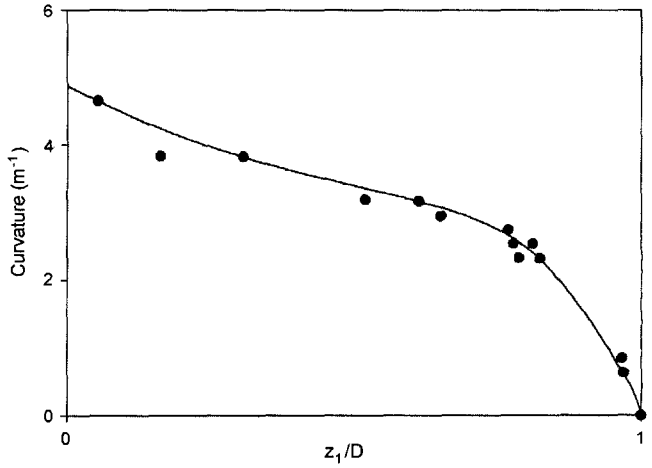

Figure 9. Curvature measured by the layer removal method.

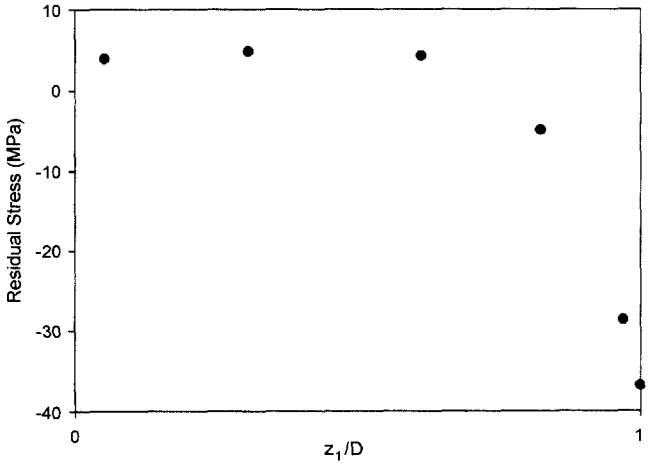

Figure 10. Residual stress distribution measured by the layer removal method.

calculated residual stress distribution is expressed at Figures 9 and 10 respectively. It has similar results to the free quenching rather than the constrained quenching; core region is under tensile mode and surface region is under compressive mode. If the friction coefficient between the polymer and the mold wall is small, it will have a similar trend to the free quenching. There is a possibility that experimental results may differ from the actual residual stress distribution in the molded part because the polymer specimen was heated by the friction between the milling cutter and the specimen, the specimen experienced compressive stress from the milling cutter and viscoelastic deformation[23] may have occurred.

Conclusions

In this study, the residual stress distribution in a semi-crystalline polymer was predicted using results of the flow field analysis. The non-Newtonian viscosity and the compressibility of the material was considered for the theoretical modelling. The pressure and temperature fields were obtained by a hybrid FEM/FDM scheme. The temperature field in the gap-wise direction was obtained by a finite difference method using coordinate transfomation to consider the moving solid-melt interface. The residual stress in the gap-wise direction was predicted from the calculated pressure and temperature fields in two cases, the free quenching and the constrained quenching. Theoretical predictions were compared with the experimental results. The layer-removal method was applied and the measured curvature data was used to calculate the residual stress distribution in the molded part. The effect of the processing conditions on the residual stress distribution was also examined.

Acknowledgements

This study was supported by research grants from the Korea Science and Engineering Foundation (KOSEF) through the Applied Rheology Center (ARC), an official KOSEF-created engineering research center (ERC) at Korea University, Seoul, Korea. The authors are grateful for the support.

References

1. G. D. Gilmore and R. S. Spencer, *Modern Plastics*, **27**(8), 143 (1950).
2. R. S. Spencer and G. D. Gilmore, *J. Colloid Sci.*, **6**, 1118 (1951).
3. C. A. Hieber and S. F. Shen, *J. Non-Newt. Fluid Mech.*, **7**, 1 (1980).
4. H. H. Chiang, C. A. Hieber, and K. K. Wang, *Polym. Eng. Sci.*, **31**, 116 (1991).
5. H. H. Chiang, C. A. Hieber, and K. K. Wang, *Polym. Eng. Sci.*, **31**, 125 (1991).
6. W. F. Zoetelief, L. F. A. Douven, and A. J. Ingen Housz, *Polym. Eng. Sci.*, **14**, 1886 (1996).
7. K. M. B. Jansen and G. Titomanlio, *Polym. Eng. Sci.*, **36**, 2029 (1996).
8. K. M. B. Jansen and G. Titomanlio, *Polym. Eng. Sci.*, **36**, 2041 (1996).
9. K. K. Kabanemi, H. Vaillancourt, H. Wang, and G. Salloum, *Polym. Eng. Sci.*, **38**, 21 (1998).
10. R. G. Treuting and W. T. Read Jr., *J. Appl. Phys.*, **22**(2), 130 (1951).
11. C. H. V. Hastenberg, P. C. Wildervanck, A. J. H. Leenen, and G. G. J. Schennink, *Polym. Eng. Sci.*, **32**, 506 (1992).
12. M. Akay and S. Ozden, *J. Mat. Sci.*, **30**, 3358 (1995).
13. M. Akay and S. Ozden, *Polym. Eng. Sci.*, **13**, 1839 (1996).
14. O. Denizart, M. Vincent, and J. F. Agassant, *J. Mat. Sci.*,

30, 552 (1995).
15. V. Leo and C. H. Cuvelliez, *Polym. Eng. Sci.*, **15**, 1961 (1996).
16. C. S. Kwok, L. Tong, and J. R. White, *Polym. Eng. Sci.*, **5**, 65 (1996).
17. K. M. B. Jansen, J. J. Orij, C. Z. Meijer, and D. J. V. Dijk, *Polym. Eng. Sci.*, **39**, 10 (1999).
18. A. I. Isayev, "Injection and Compression Molding Fundamentals", Marcel Dekker, New York, 1987.
19. S. C. Lee and J. R. Youn, *J. Reinf. Plas. Comp.*, **18**, 186 (1999).
20. J. H. Jung, S. W. Lee, and J. R. Youn, *Macromolecular Symposia*, **148**, 263 (1999).
21. Y. I. Kwon, M. S. Thesis, Seoul National University, Seoul, 1999.
22. J. Crank, "Free and Moving Boundary Problems", pp. 163-282, Clarendon Press, Oxford, 1987.
23. H. See, *Korea-Australia Rheology J.*, **13**, 67 (2001).